Characterization of a unique [FeS] cluster in the electron transfer chain of the oxygen tolerant [NiFe] hydrogenase from *Aquifex aeolicus*

Maria-Eirini Pandelia[a], Wolfgang Nitschke[b], Pascale Infossi[b], Marie-Thérèse Giudici-Orticoni[b], Eckhard Bill[a], and Wolfgang Lubitz[a,1]

[a]Max-Planck-Institut für Bioanorganische Chemie, Stiftstrasse 34-36, D-45470 Mülheim a.d. Ruhr, Germany; and [b]Laboratoire de Bioénergétique et Ingénierie des Protéines, Mediterranean Institute of Microbiology, 13402 Marseille Cedex 20, France

Edited by Harry B. Gray, California Institute of Technology, Pasadena, CA, and approved February 23, 2011 (received for review January 13, 2011)

Iron-sulfur clusters are versatile electron transfer cofactors, ubiquitous in metalloenzymes such as hydrogenases. In the oxygen-tolerant Hydrogenase I from *Aquifex aeolicus* such electron "wires" form a relay to a diheme cyt*b*, an integral part of a respiration pathway for the reduction of O_2 to water. Amino acid sequence comparison with oxygen-sensitive hydrogenases showed conserved binding motifs for three iron-sulfur clusters, the nature and properties of which were unknown so far. Electron paramagnetic resonance spectra exhibited complex signals that disclose interesting features and spin-coupling patterns; by redox titrations three iron-sulfur clusters were identified in their usual redox states, a [3Fe4S] and two [4Fe4S], but also a unique high-potential (HP) state was found. On the basis of ^{57}Fe Mössbauer spectroscopy we attribute this HP form to a superoxidized state of the [4Fe4S] center proximal to the [NiFe] site. The unique environment of this cluster, characterized by a surplus cysteine coordination, is able to tune the redox potentials and make it compliant with the $[4Fe4S]^{3+}$ state. It is actually the first example of a biological [4Fe4S] center that physiologically switches between 3+, 2+, and 1+ oxidation states within a very small potential range. We suggest that the (1+/2+) redox couple serves the classical electron transfer reaction, whereas the superoxidation step is associated with a redox switch against oxidative stress.

electrochemistry | EPR | iron-sulfur centers | O_2-sensitivity

Hydrogenases are metalloproteins occurring in the metabolic pathway of a wide variety of microbial organisms and catalyze the reversible oxidation of dihydrogen: $H_2 \rightleftharpoons 2H^+ + 2e^-$ (1). The growing interest in alternative sources of energy has focused scientific research on understanding and engineering these enzymes for future applications (2). One of the major limitations of hydrogenases, however, is their sensitivity towards oxygen. Recently, the discovery of hydrogenases that retain catalytic activity in oxygenic environments has potentially opened new applications as "green" vanguard catalysts, in particular as electrocatalysts on electrodes for biofuel cells (3, 4).

Aquifex aeolicus is a hyperthermophilic Knallgas bacterium with optimum growth temperature of 85 °C (5). This microorganism harbors three distinct [NiFe] hydrogenases, among which Hase I is located in the aerobic respiration pathway and attached to the membrane *via* a diheme cyt*b* (6). Hase I consists of two subunits; the large subunit contains the hetero-bimetallic nickel-iron site and the small subunit the electron transfer cofactors, namely iron-sulfur clusters (6). Based on spectroelectrochemical studies, this enzyme exhibits enhanced thermostability and tolerance for inhibitors (e.g., O_2 and CO) (4, 7).

Although the structures of O_2-sensitive hydrogenases are well characterized (8, 9), such information is still lacking for O_2-tolerant enzymes. The molecular mechanism and structural determinants for this increased oxygen tolerance remain to be understood. Recent EPR and FTIR studies have shown that the [NiFe] center of Hase I has a geometric and electronic structure similar to standard hydrogenases (6, 7). The as-isolated enzyme is in the Ni-B state, a dormant form known to carry a bridging hydroxyl ligand between the two metals. The Ni-B state is quickly reactivated and Hase I enters the catalytic cycle consisting of three intermediates (7). Reactivation occurs at potentials similar to those of standard hydrogenases, whereas catalysis sets in at approximately 100 mV more positive potentials (7).

In standard [NiFe] hydrogenases electrons are channeled to the redox partners through a "wire" consisting of one [3Fe4S] cluster placed in-between two low-potential [4Fe4S] clusters (8) (Fig. 1). In the sequence of the small subunit of Hase I, the ten cysteines and one histidine that bind these three iron-sulfur centers are fully conserved, indicating that one [3Fe4S] and two [4Fe4S] clusters are also present in Hase I (Fig. 1). The EPR signals of these clusters, however, are more complex (6) than in standard hydrogenases, showing additional species and magnetic interactions (10).

A closer inspection of the iron-sulfur center proximal to the [NiFe] active site and homology structure models show that the latter has an atypical sequence motif $CX\underline{C}\underline{C}X_{94}CX_4\underline{C}X_{28}C$, with two extra cysteines ($\underline{C}$); these may potentially participate in its coordination and thus affect its electronic and redox properties. Interestingly these extra cysteines are also present in the membrane bound hydrogenase (MBH) from *Ralstonia eutropha* and Hyd-1 from *Escherichia coli* (Fig. 1), which show similar spectroscopic features (11, 12). The presence of these residues has been shown to contribute to the oxygen stability of the *R. eutropha* enzyme and is therefore associated with a possible redox chemistry protecting the enzyme against oxidative stress (13). In the present work the type and redox properties of the constituent iron-sulfur clusters are investigated with the aim to (*i*) portray the energy coupled processes between Hase I and its redox partners and (*ii*) outline a relation between O_2-tolerance and electronic/chemical events occurring at the iron-sulfur clusters.

Results

At low temperatures (<55 K) the continuous wave (cw) X-Band EPR spectrum of the as-isolated Hase I from *A. aeolicus* exhibits complex spectral features in the region, where an almost isotropic signal at $g = 2.02$ from an oxidized $[3Fe4S]^+$ ($S = 1/2$) is observed in standard hydrogenases (Fig. 2, dashed line, Table S1) (6, 14). Double integration of the iron-sulfur cluster signals accounted for 1.9 ± 0.3 spins/mol of protein, indicating the presence of two $S = 1/2$ centers. In the case of magnetically

Author contributions: M.-E.P., M.T.G.-O., and W.L. designed research; M.-E.P., W.N., and E.B. performed research; W.N., P.I., and M.T.G.-O. contributed new reagents/analytic tools; M.-E.P., W.N., and E.B. analyzed data; and M.-E.P. and W.L. wrote the paper.

The authors declare no conflict of interest.

This article is a PNAS Direct Submission.

[1]To whom correspondence should be addressed. E-mail: lubitz@mpi-muelheim.mpg.de.

This article contains supporting information online at www.pnas.org/lookup/suppl/doi:10.1073/pnas.1100610108/-/DCSupplemental.

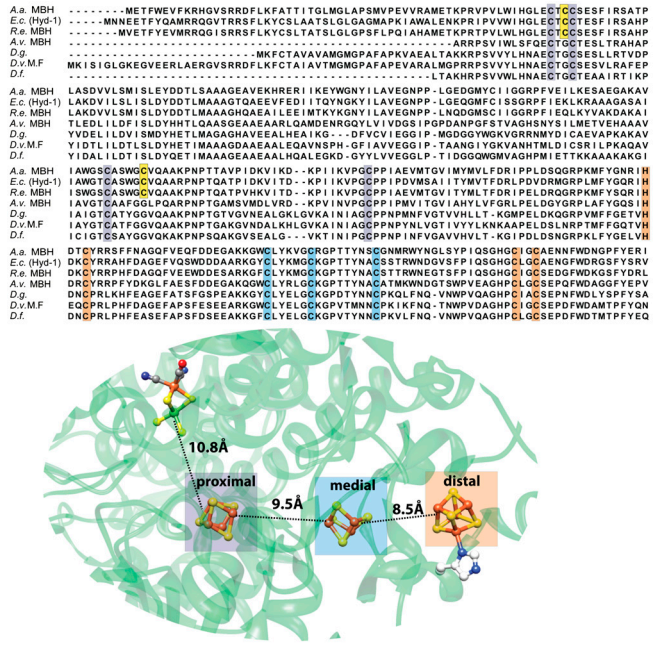

Fig. 1. Top: Sequence alignment of O_2-sensitive and O_2-tolerant hydrogenases. A set of columns of the same color represents the conserved residues that bind a specific cluster, highlighted in the structure of *D. vulgaris* MF (1WUI pdb code). The two extra cysteines in the *A. aeolicus* enzyme are depicted in yellow. Bottom: Localization of the [NiFe] site and the three [FeS] clusters in the standard hydrogenases and the closest metal-to-metal distances between different cofactors. The [FeS] clusters are denoted as proximal (P), medial (M), and distal (D), based on their distance from the [NiFe] site (Fig.S1).

noninteracting species, their EPR signals appear at the same positions on a g-factor scale at different microwave frequencies. In Hase I, however, these multiline patterns are different for the spectra recorded at S-, X-, and Q-band frequencies (Fig. 2, Fig. S2). This dependence argues for spin-spin interactions between these two species with exchange and dipolar contributions (10, 15, 16). Such magnetic interactions can be observed in cw EPR spectra between paramagnetic centers localized less than 15 Å apart, suggesting that these centers in Hase I are adjacent to each other (17) (Fig. 1). In addition, the splitting patterns of these EPR spectra show that the exchange interaction lies in an intermediate range ($|2J| \approx \Delta g \mu_B B$) (15, 16). Furthermore, there could be an additional interaction with the paramagnetic [NiFe] center ($S = 1/2$), see below. The relaxation of all components of the spectrum has very similar temperature dependence between 10 and 50 K (Fig. S3); above 50 K all signals are broadened beyond detection.

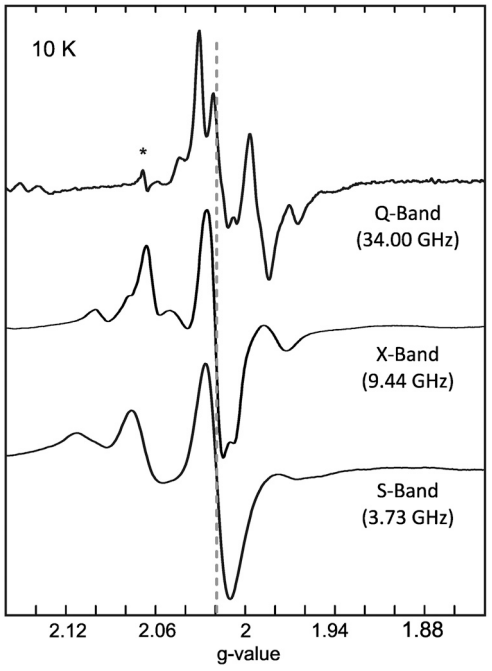

Fig. 2. EPR spectra of the [FeS] clusters in the as-isolated state of Hase I (pH 7.4) at S-band (cw), X-band (cw), and Q-Band (pulse) frequencies at $T = 10$ K. The asterisk marks a cavity impurity. The dashed line denotes the position of the $[3Fe4S]^{1+}$ signal. Experimental Conditions: Modulation amplitude 0.3 mT and 1 mT; mw power 6 mW and 2 mW for S- and X-band, respectively.

EPR Redox Titration (pH 7.4). To unravel the complex features in the EPR spectra of Hase I and identify the contributions from the individual [FeS] clusters, potentiometric titrations were carried out. Selected spectra illustrating all detectable iron-sulfur centers are shown for pH 7.4 in Fig. 3. The initial working hypothesis is that three iron-sulfur cofactors are expected to yield three single-electron redox transitions.

As shown in Fig. 3 *A–D* the spectral patterns of the iron-sulfur clusters are drastically changing with redox potential allowing the identification of four groups of EPR signals, corresponding to interacting paramagnetic centers. By monitoring the intensity of these complex patterns *four* distinct one-electron transitions related to the iron-sulfur clusters of Hase I (Fig. 3*E*) could be identified (Table 1). The pH-dependence of these redox transitions has also been examined (Table S2). Considering our initial hypothesis, there appears to be a contradiction with respect to the number of redox centers available and the number of observed redox transitions.

Assignment of the [FeS] Clusters. The $[3Fe4S]^{1+}$ cluster can be assigned in a straightforward way on the basis of its *g*-value ($g_{iso} = 2.019$) to the signal denoted as 2 (Fig. 3). For the remaining [FeS] centers identification is more difficult as their assignments require knowledge of the structure and interaction patterns. Therefore, an additional species that could be linked to these spectral features and used as a probe to identify the localization of these centers is required. This information can be obtained by observing the magnetic interaction with the paramagnetic [NiFe] center.

The most oxidized Ni-B state of the [NiFe] center has a rhombic EPR spectrum ($g_x = 2.30$, $g_y = 2.17$, and $g_z = 2.01$) (7). In standard hydrogenases, reduction of the iron-sulfur cluster proximal to the [NiFe] site, induces a splitting of the nickel signals and was previously characterized to result from spin exchange and magnetic dipole-dipole interactions (15). In Hase I, reduction of the [4Fe4S] cluster denoted as 3 (Fig. 3 *B* and *C*) is accompanied by the formation of a "splitting" of the Ni-B signals (Fig. 4*A*), indicative of a magnetic interaction between these two centers (15, 17). When the sample is annealed to 80 K the uncoupled EPR spectrum of the Ni-B state is recovered, due to the faster relaxation of [FeS] clusters at such temperatures (Fig. 4*B*). The EPR signal 3 in Hase I is thus assigned to the $[4Fe4S]^{1+}$ cluster proximal to the [NiFe] site (Fig. 1). Each principal *g*-value of the Ni-B spectrum is split symmetrically into two components of comparable amplitude (18), showing that the exchange interaction between the [NiFe] site and the [4Fe4S] cluster is weak ($|2J| << \Delta g \mu_B B$) (15). The spectrum in Fig. 4*A* has been simulated with the spin Hamiltonian described in the *SI Text*, taking into account three interacting species (Ni-B, $[4Fe4S]_P$, and $[3Fe4S]_M$). The magnitude of the isotropic exchange between the [NiFe] site and the proximal tetranuclear [FeS] cluster ($J_{NiB\text{-}P}$) is 36×10^{-4} cm^{-1}, while the isotropic exchange between the proximal and medial clusters ($J_{P\text{-}M}$) is 7×10^{-4} cm^{-1}.

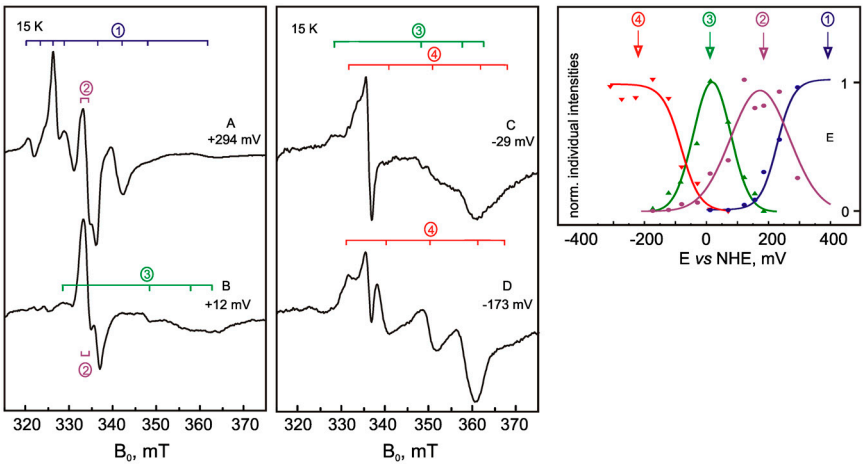

Fig. 3. (*A*, *B*, *C*, and *D*) cw X-Band EPR spectra of the EPR signals corresponding to the [FeS] clusters of Hase I at different potentials (9.433 GHz, 15 K) and (*E*) their redox titration as a function of the potential at pH 7.4. The normalized individual EPR intensities of all redox components are plotted against the redox potential and fitted to curves calculated from the Nernst equation corresponding to single-electron transitions. Mod. amplitude 1 mT, mw power 2 mW.

At potentials as low as −29 mV, the spectral features of the proximal $[4Fe4S]^{1+}$ cluster decrease in intensity and more composite signals appear (signals denoted as 4, Fig. 3) that correspond to the one-electron reduction of another [FeS] center. This center has the most reducing potential and is assigned to the distal $[4Fe4S]^{1+}$ cluster (18–20). On the basis of homology model structures of Hase I, the distance between proximal and distal clusters is similar to the one in standard hydrogenases (Fig. 1, Fig. S1) and is too large for these two species to exhibit magnetically coupled EPR spectra (17). Therefore, the complex signals are attributed to an interaction pattern of the two reduced proximal and distal clusters (S=1/2) mediated by the high spin $[3Fe4S]^{0}$ cluster ($S = 2$). These signals are well resolved in contrast to the broad and featureless spectrum of the reduced iron-sulfur clusters in standard hydrogenases (14, 15, 18, 19) (Fig. S6).

Identification of the HP Species. Fig. 5 shows spectra of Hase I poised at different positive potentials between +44 and +346 mV at pH 6.4. At mildly reducing conditions (+44 mV) the proximal [4Fe4S] is reduced and is magnetically coupled to the [NiFe] site leading to a splitting of the Ni-B EPR signal. At +176 mV the signal of the proximal iron-sulfur cluster disappears due to its oxidation to the 2+ state ($S = 0$) and, concomitantly, the Ni-B signal attains its "unsplit" form. The $[3Fe4S]^{1+}$ cluster is too far away from the [NiFe] site (~18 Å) to induce interaction fingerprints on the Ni-B signals.

Unexpectedly, an additional redox transition occurs at higher redox potentials, assigned to a high-potential (HP) species denoted as 1 (Fig. 3*E*); at +346 mV the Ni-B components are broadened and shifted and exhibit an astonishing relaxation enhancement. In addition, the $[3Fe4S]^{1+}$ signal is now converted into a more complex pattern (Fig. 5). These spectral features show that the paramagnetic HP species must be positioned sufficiently close to both the [NiFe] and the [3Fe4S] cluster to allow magnetic interactions. The HP center is thus identified as the proximal iron-sulfur cluster lying in between these centers (8, 15, 17), implying that it has become oxidized to the 3+ state.

The proximal cluster in Hase I thus undergoes two distinct one-electron transitions ($HP \overset{e^-}{\rightleftharpoons} [4Fe4S]^{2+} \overset{e^-}{\rightleftharpoons} [4Fe4S]^{1+}$). Both, the superoxidized and reduced forms of the proximal cluster are spin coupled with the [NiFe] site (Fig. 5), however, the magnitude of interaction is markedly different. At very oxidizing potentials the isotropic exchange coupling is in the intermediate range. Measurements at W-Band frequencies (~94 GHz) set the upper limit for the interaction of the HP species with the [NiFe] site to be $0.021(2)$ cm^{-1} consistent with the significant relaxation enhancement observed for the Ni-B signals (Fig. S7, Fig. S8, Fig. S9, Fig. S10). In contrast, the exchange coupling between the $[4Fe4S]^{1+}$ species and the Ni-B state of the [NiFe] site is about an order of magnitude weaker ($0.0036(3)$ cm^{-1}) (Fig. S9, Fig. S10).

Electronic Properties and Characterization of the HP Species. The proximal cubane cluster is able to participate in two successive redox transitions implying that this center can be oxidized to a (3+) state (21). W-Band EPR shows that this HP species has a very small g-anisotropy, in contrast to a typical high-potential iron-sulfur (HiPIP) center (22) (Fig. S8, Fig. S9). The small g-anisotropy, however, could represent a different valence delocalization on this cluster, affecting the ground state properties and yielding different *g*-factors. The relaxation properties of the HP center resemble an iron-sulfur cluster rather than a radical signal (Fig. S2), excluding the possibility that the spin is localized on a ligand (e.g., covalently bound to a $[4Fe4S]^{2+}$ moiety) (23).

Therefore, ^{57}Fe Mössbauer experiments have been performed on the as-isolated and the fully oxidized Hase I to ascertain the oxidation state of the proximal cluster in the HP state. The analysis first corroborated the presence of a three-iron and two four-iron clusters. Fig. 6 shows the Mössbauer spectrum of the as-isolated enzyme recorded at zero magnetic field. This spectrum differs

Table 1. Apparent midpoint potentials of the iron-sulfur clusters in O_2-sensitive and O_2-tolerant enzymes

Redox center	Apparent midpoint potential, mV				
	A. aeolicus (this work)	*R. eutropha* H16 / *R. metallidurans* CH34 (28)	*D. vulgaris* MF (14)	*D. gigas* (19)	*D. fructosovorans* (18)
HP	+ 232	+160/ + 240	–	–	–
$[3Fe4S]^{1+/0}$ (medial)	+ 68	+25/ + 100	− 70	−35, − 70	+ 65
$[4Fe4S]^{2+/1+}$ (proximal)	+ 87	−60/ + 50	< − 300	− 290	− 340
$[4Fe4S]^{2+/1+}$ (distal)	− 78	−180/ − 80	< − 300	− 340	− 340

Values are quoted relative to the normal hydrogen electrode (NHE). The error is ±20 mV (for *A. aeolicus*).

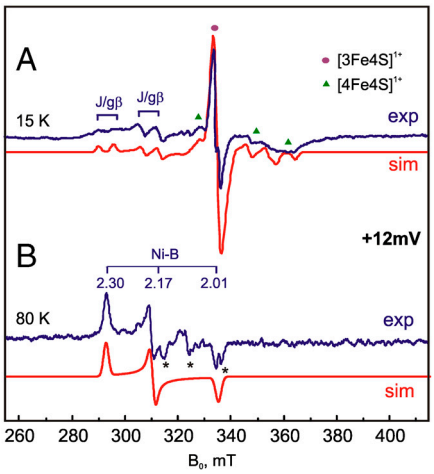

Fig. 4. cw X-Band EPR spectra at +12 mV and their simulations at 15 (*A*) and 80 K (*B*) are shown for pH 7.4. The asterisks denote cavity or undetermined signals. Mod. amplitude 1 mT, mw power 2 mW (15 K) and 20 mW (80 K) at 9.433 GHz.

from the one reported for standard hydrogenases (10, 19) by two main features: (*i*) a substantially higher amount of Fe^{3+} that can be best ascribed to oxidation of the proximal cluster from the (2+) state with average valence $Fe^{2.5+}$ to the (3+) state and (*ii*) a subspectrum with an isomer shift of 0.46 mms^{-1} and an unusually large quadrupole splitting $\Delta E_Q = 2.41$ mms^{-1} (Table S3). The latter indicates a special Fe subsite with an additional coordinating ligand in a distorted geometry (24–26). The average isomer shift for this cluster in this state is $\delta_{av} = 0.34$ mms^{-1} at 160 K, being in the range of those reported for HiPIP-like cubane clusters (22).

Discussion

The Redox Potentials of the Three [FeS] Clusters. The components of the electron transfer chain in Hase I and their redox potentials have been determined and compared to those occurring in other homologous hydrogenases (Table 1). The distal $[4Fe4S]^{2+/1+}$ cluster has a reduction potential of −78 mV that is pH-dependent

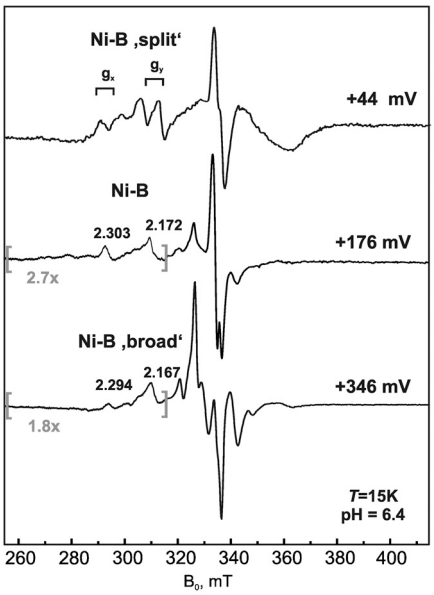

Fig. 5. cw X-Band EPR spectra at pH 6.4 poised at +44, +176, and +346 mV ambient redox potentials. The low-field regions between the gray brackets have been amplified. Mod. amplitude 1 mT, mw power 2 mW at 9.436 GHz and $T = 15$ K.

(20). The estimated $pK_{a(ox)}$ is 7.1 and may be attributed to the protonation of the histidine ligand of this cluster (8, 18). The midpoint potential of the distal [FeS] cluster is approximately 300 mV more positive than the one in standard hydrogenases, which can be rationalized in terms of the higher potential redox partner of Hase I, a diheme cyt*b* ($E_m = -20$, −110 mV) (27).

The medial $[3Fe4S]^{1+/0}$ cluster is found to have a reduction potential of +68 mV. There is a large variation in the values reported for the medial clusters in standard and O_2-tolerant hydrogenases (Table 1) (14, 18, 19, 28). In general, in O_2-tolerant hydrogenases there is a trend towards more positive potentials that may be related to the surrounding of this cluster. In the pH range between 6.4 and 8.3, the midpoint potential for the [3Fe4S] is independent of the proton concentration, in agreement with previous results on O_2-sensitive enzymes (20).

The proximal cluster is able to access three redox states: $[4Fe4S]^{3+}$ (HP state), $[4Fe4S]^{2+}$, and $[4Fe4S]^{1+}$. The $[4Fe4S]^{3+/2+}$ couple has a reduction potential of +232 mV that is essentially pH-independent in the range between 6.4 and 7.4. Such a high-potential species is so far found only in O_2-tolerant hydrogenases (Table 1), suggesting its possible role in protection against O_2-inactivation. The second $[4Fe4S]^{2+/1+}$ redox couple of the proximal cluster has an apparent midpoint potential of +87 mV, which is about +300 to +440 mV more positive than the respective ones for the hydrogenases from *Desulfovibrio* and *Allochromatium* species (10, 18–20). Such a very positive potential is not entirely atypical for $[4Fe4S]^{2+/1+}$ centers. In the MBH hydrogenases from *R. eutropha* H16 and *R. metallidurans* CH34, the reduction potential for this cluster is also very positive (28, 29), while in the nitrate reductase from *E. coli,* both [3Fe4S] and [4Fe4S] clusters have comparable reduction potentials with those in Hase I (29). For pH values greater than 7.4 the E_m of the $[4Fe4S]^{2+/1+}$ couple approaches a dependence of 57 mV/pH and the proton association constant inferred is between 6.9 and 7.1 (Fig. S5), indicating a proton-coupled electron transfer involving a coordinating residue of this cluster.

The Dual Redox Character of the Proximal Cluster. The proximal cluster in Hase I allows two redox transitions (i.e., 3 + /2+, 2 + /1+), which usually are mutually exclusive and do not occur in biological systems. This high redox compliance is proposed to be related to an unusual ligation by five or six cysteines, as may be inferred from homology modeling. Such additional thiol ligand(s) can easily alter the cluster geometry as well as the redox properties (24, 26, 30).

Also, oxidation of cysteines to disulfides has been associated with a protective mechanism against reactive oxygen species (31). Such a chemistry could be similar to that of the Ferredoxin:Thioredoxin Reductase (FTR) (32) and the heterodisulfide reductase (HDR) (33), in which a [4Fe4S] cluster mediates the cleavage of a disulfide. If in a similar manner formation of a disulfide bridge would occur upon the one-electron oxidation of the proximal cluster to the HP state, the cluster should be *reduced*, because bond formation is a two-electron process. However, this scheme disagrees with the present Mössbauer experiments that show iron *oxidation*. Moreover, formation of a disulfide bridge would presumably rupture the Fe-S bond at that site and affect the cluster stability.

A more likely possibility is that one or more of these additional cysteines are capable of coordinating the proximal [4Fe4S] cluster. A similar situation has been observed for the *N*-ethylmaleimide (NEM)-modified FTR that represents the only biological example of a $[4Fe4S]^{3+}$, in which one Fe is coordinated by two cysteine residues (32, 34, 35). The large quadrupole splitting assigned to one of the Fe ions of this cluster in Hase I is indicative of a unique subsite with two-coordinating protein ligands in a distorted geometry that deviates from the conventional quasitetrahedral symmetry. Such high coordination leads to a large

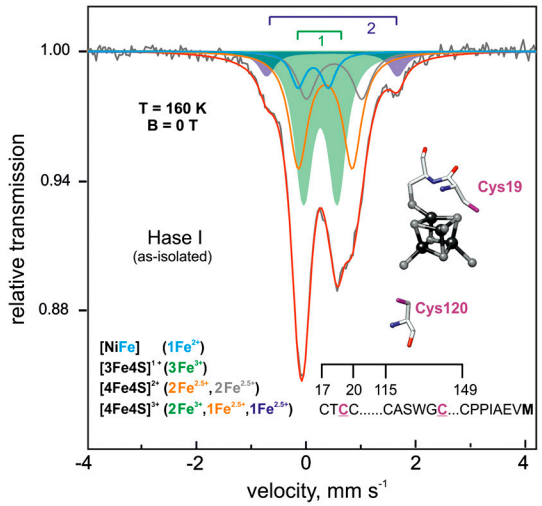

Fig. 6. ^{57}Fe Mössbauer spectrum of the as-isolated Hase I at pH 7.4 recorded at $T = 160$ K without applied magnetic field. The spectrum can be well fitted accounting for a $[3Fe4S]^{1+}$, a $[4Fe4S]^{2+}$, a low-spin Fe^{2+} of the [NiFe] site, and a $[4Fe4S]^{3+}$ with a special site. The doublet 1 indicates the ferric contribution in the spectrum and the doublet 2 the Fe site with the large quadrupole splitting. The structure of the modeled proximal cubane cluster with the additional cysteine residues is shown. The spectra are deconvoluted to the respective components, whose contributions are indicated by the color of the doublets.

quadrupole splitting for the distorted Fe subsite and shifts the $3+/2+$ reduction potential of the HiPIP-like core to lower values, as has been shown for synthetic five-coordinated [FeS] cubanes (24). The latter originates from the increased negative charge of the cluster, which in biological systems, however, may be partially counterbalanced by additional hydrogen bonds leading overall to less covalent Fe-S bonds (30, 36). In addition, synthetic five-coordinated clusters can also carry out two redox steps in a close range of potentials. However, in contrast to the case of Hase I, the oxidation products in synthetic clusters are unstable and the transitions are often irreversible (24, 26).

The proximal [FeS] cubane shuttles reversibly through three different oxidation states in a very small potential range (~150 mV). Up to date, attempts to overoxidize a $[4Fe4S]^{1+}$ cluster resulted in loss of an iron, whereas reversible superreduction of $[4Fe4S]^{3+}$ clusters is possible but the potential range between the $[4Fe4S]^{3+}$ and the $[4Fe4S]^{1+}$ spans more than 1,000 mV (37). The ability of the proximal cluster in Hase I to carry out two single-electron transitions is rather unusual. From the Mössbauer experiments this cluster is shown to have a unique Fe subsite in a distorted coordination environment indicating that this is coordinated by two cysteine residues (24–26). Such coordination should lead to an enhancement in the electron donation from the ligands to the iron-sulfur cluster core, particularly to molecular orbitals that have metal character and are slightly antibonding (34). The enhanced ligand-to-metal donation should result in an elongation of Fe-Fe distances and to a more distorted structure of the proximal [FeS] cluster (Fig. S11). Because stability of five or six coordinated clusters relates to the presence of terminal thiol ligands (24, 26), there may also be an active role for the second additional cysteine, as demonstrated in recent mutation experiments (13). The presence of the second additional cysteine is thus likely to be important for the stability of the induced HiPIP-like core.

Implications for Oxygen Tolerance. The first redox transition $(2+/1+)$ of the proximal cluster serves in the canonical electron transfer reaction of the enzyme and its midpoint potential is far more positive as compared to the ones reported for standard hydrogenases. This upshift in the reduction potential is expected to result from an adaptation of the whole electron transfer chain to the more positive final electron acceptor (quinone as compared to cytc_3). As a consequence, the [FeS] cofactors in Hase I are poor electron donors for oxidizing species (i.e., O_2) and thus render the enzyme partially O_2-tolerant. The second transition of the proximal cluster $(3+/2+)$ appears to be associated with a redox switch against oxidative stress rather than participating in the catalytic function of the enzyme. An increase in O_2-sensitivity was reported in mutagenesis experiments of the additional cysteines surrounding the proximal cluster in *R. eutropha* MBH (13). It is intriguing to understand the presence of easily oxidizable cysteines in enhancing the oxygen tolerance of a hydrogenase, because these could readily react with O_2. Formation of disulfide bonds could protect against oxidative stress but on the other hand also increase the generation of reactive oxygen species. This scenario is not supported by the present Mössbauer experiments.

It is not clear how oxygen diffuses in and interacts with Hase I, and whether there is a specific sequence of oxidation events following its interaction with the metal centers in their different redox states. Nevertheless, O_2-tolerance of enzymes such as Hase I is understood to comprise a concerted effect of redox (thermodynamic) and kinetic factors (7, 38). Considering the redox potentials of the "activated" [NiFe] site and the reduced [FeS] clusters (7), the [NiFe] site is likely to be the primary target of O_2. It is assumed that reduction of the attacking O_2 molecules then proceeds *via* electrons supplied from the [NiFe] site that are also delivered from oxidation of the [FeS] clusters. Models for these reactions have been proposed (38). In this sense, the proximal cluster may represent a cofactor that is situated sufficiently close so that it can provide an additional reducing equivalent by forming the superoxidized state, for efficient neutralization of reactive oxygen species at the active site (38). The occurrence of two redox transitions for the proximal cluster, of which at least one is coupled to a proton transfer, contributes but is not solely responsible for the observed O_2-tolerance (13) of membrane bound hydrogenases harboring these two extra cysteines. In conclusion and following the scheme proposed earlier for O_2 inactivation (38), it is suggested that in enzymes such as Hase I from *A. aeolicus* the superoxidized state of the proximal cluster promoted by its cysteine surplus coordination is a key intermediate in a protection reaction against attack by molecular oxygen.

Materials and Methods

Detailed descriptions are available in *SI Text*.

The hyperthermophilic bacterium *A. aeolicus* was grown at 85 °C in two-liter bottles under a $CO_2/H_2/O_2$ atmosphere. Hydrogenase I was purified at room temperature under semianaerobic conditions in a 50 mM Tris-HCl buffer pH 7.0, in the presence of 5–10% glycerol and 0.01% n-dodecyl-β-D-maltoside (DDM) as previously described (6). Redox potentials were determined by cw EPR potentiometric titrations. The titration was carried out anaerobically by adjusting the potential with substoichiometric amounts of solutions of sodium dithionite ($Na_2S_2O_4$) and potassium ferricyanide ($K_3[Fe(CN)_6]$).

ACKNOWLEDGMENTS. The authors are grateful to Dr. Thomas Weyhermüller (MPI Mülheim) and Dr. Oliver Lenz (HU Berlin) for helpful discussions. This work was supported by EU/Energy Network project SOLAR-H2 (FP7 Contract 212508), Bundesministerium für Bildung and Forschung (BMBF) (03SF0318B, 03SF0355C), Max Planck Society, CNRS, French National Research Agency, the city of Marseilles, Région Provence-Alpes-Côte d'Azur, "Pôle de compétitivité CapEnergies.

1. Cammack R, Frey M, Robson R (2001) *Hydrogen as a fuel: learning from Nature* (Taylor and Francis, London).

2. Mertens R, Liese A (2004) Biotechnological applications of hydrogenases. *Curr Opin Biotech* 15:343–348.

3. Vincent KA, et al. (2005) Electrocatalytic hydrogen oxidation by an enzyme at high carbon monoxide or oxygen levels. *Proc Natl Acad Sci USA* 102:16951–16954.
4. Luo XJ, Brugna M, Tron-Infossi P, Giudici-Orticoni MT, Lojou E (2009) Immobilization of the hyperthermophilic hydrogenase from *Aquifex aeolicus* bacterium onto gold and carbon nanotube electrodes for efficient H_2 oxidation. *J Biol Inorg Chem* 14:1275–1288.
5. Deckert G, et al. (1998) The complete genome of the hyperthermophilic bacterium *Aquifex aeolicus*. *Nature* 392:353–358.
6. Brugna-Guiral M, et al. (2003) [NiFe] hydrogenases from the hyperthermophilic bacterium *Aquifex aeolicus*: properties, function, and phylogenetics. *Extremophiles* 7:145–157.
7. Pandelia ME, et al. (2010) Membrane-bound hydrogenase I from the hyperthermophilic bacterium *Aquifex aeolicus*: enzyme activation, redox intermediates and oxygen tolerance. *J Am Chem Soc* 132:6991–7004.
8. Volbeda A, et al. (1995) Crystal structure of the nickel-iron hydrogenase from *Desulfovibrio gigas*. *Nature* 373:580–587.
9. Fontecilla-Camps JC, Volbeda A, Cavazza C, Nicolet Y (2007) Structure/function relationships of [NiFe]- and [FeFe]-hydrogenases. *Chem Rev* 107:4273–4303.
10. Surerus KK, et al. (1994) Further characterization of the spin coupling observed in oxidized Hydrogenase from *Chromatium vinosum*. A Mössbauer and multifrequency EPR Study. *Biochemistry* 33:4980–4993.
11. Saggu M, et al. (2009) Spectroscopic insights into the oxygen-tolerant membrane-associated [NiFe] hydrogenase of *Ralstonia eutropha* H16. *J Biol Chem* 284: 16264–16276.
12. Lukey MJ, et al. (2010) How *Escherichia coli* is equipped to oxidize Hydrogen under different redox conditions. *J Biol Chem* 285:3928–3938.
13. Lenz O, et al. (2010) H_2 conversion in the presence of O_2 as performed by the membrane-bound [NiFe]-hydrogenase of *Ralstonia eutropha*. *ChemPhysChem* 11:1107–1119.
14. Asso M, Guigliarelli B, Yagi T, Bertrand P (1992) EPR and redox properties of *Desulfovibrio vulgaris* Miyazaki hydrogenase-comparison with the NiFe enzyme from *Desulfovibrio gigas*. *Biochim Biophys Acta* 1122:50–56.
15. Guigliarelli B, et al. (1995) Structural organization of the Ni and (4Fe-4S) centers in the active form of *Desulfovibrio gigas* hydrogenase. Analysis of the magnetic-interactions by Electron Paramagnetic Resonance spectroscopy. *Biochemistry* 34:4781–4790.
16. Bencini A, Gatteschi D (1990) *Electron Paramagnetic Resonance of Exchange Coupled Systems* (Springer-Verlag New York, Inc, New York).
17. Coffman RE, Buettner GR (1979) General magnetic dipolar interaction of spin-spin coupled molecular dimers—application to an EPR spectrum of xanthine oxidase. *J Phys Chem* 83:2392–2400.
18. Rousset M, et al. (1998) [3Fe-4S] to [4Fe-4S] cluster conversion in *Desulfovibrio fructosovorans* [NiFe] hydrogenase by site-directed mutagenesis. *Proc Natl Acad Sci USA* 95:11625–11630.
19. Teixeira M, et al. (1989) Redox intermediates of *Desulfovibrio gigas* [NiFe] hydrogenase generated under hydrogen—Mössbauer and EPR characterization of the metal centers. *J Biol Chem* 264:16435–16450.
20. Roberts LM, Lindahl PA (1995) Stoichiometric reductive titrations of *Desulfovibrio gigas* hydrogenase. *J Am Chem Soc* 117:2565–2572.
21. Beinert H, Holm RH, Münck E (1997) Iron-sulfur clusters: nature's modular, multipurpose structures. *Science* 277:653–659.
22. Bertini I, Campos AP, Luchinat C, Teixeira M (1993) A Mössbauer investigation of oxidized Fe4S4 HiPIP II from *Ectothiorhodospira halophila*. *J Inorg Biochem* 52:227–234.
23. Hu ZG, Jollie D, Burgess BK, Stephens PJ, Münck E (1994) Mössbauer and EPR Studies of *Azotobacter vinelandii* Ferredoxin-I. *Biochemistry* 33:14475–14485.
24. Ciurli S, et al. (1990) Subsite-differentiated analogs of native $[4Fe\text{-}4S]^{2+}$ clusters—preparation of clusters with 5-coordinate and 6-coordinate subsites and modulation of redox potentials and charge distributions. *J Am Chem Soc* 112:2654–2664.
25. Johnson RE, Papaefthymiou GC, Frankel RB, Holm RH (1983) Effects of secondary bonding interactions on the $[Fe_4S_4]^{2+}$ core of ferredoxin site analogs—$Fe_4S_4(SC_6H_4 - o - OH)_4]^{2-}$, a distorted cubane-type cluster with one five-coordinate iron atom. *J Am Chem Soc* 105:7280–7287.
26. Kanatzidis MG, Coucouvanis D, Simopoulos A, Kostikas A, Papaefthymiou V (1985) Synthesis, structural characterization, and electronic properties of the tetraphenylphosphonium salts of the mixed terminal ligand cubanes $Fe_4S_4(Et_2Dtc)_n(X)_{4n}^{2-}$ ($X = Cl^-$, PhS^-) ($n = 1$, 2). Two different modes of ligation on the $[Fe_4S_4]^{2+}$ core. *J Am Chem Soc* 107:4925–4935.
27. Infossi P, et al. (2010) *Aquifex aeolicus* membrane hydrogenase for hydrogen biooxidation: role of lipids and physiological partners in enzyme stability and activity. *Int J Hydrogen Energy* 35:10778–10789.
28. Knüttel K, et al. (1994) Redox properties of the metal centers in the membrane-bound hydrogenase from *Alcaligenes eutrophus* CH34. *Bull Pol Acad Sci Chem* 42:495–511.
29. Guigliarelli B, et al. (1992) EPR and redox characterization of iron-sulfur centers in nitrate reductases-A and Z- from *Escherichia-coli*. Evidence for a high-potential and a low-potential class and their relevance in the electron-transfer mechanism. *Eur J Biochem* 207:61–68.
30. Dey A, et al. (2007) Solvent tuning of electrochemical potentials in the active sites of HiPIP versus Ferredoxin. *Science* 318:1464–1468.
31. Vita N, Hatchikian EC, Nouailler M, Dolla A, Pieulle L (2008) Disulfide bond-dependent mechanism of protection against oxidative stress in pyruvate-ferredoxin oxidoreductase of anaerobic *Desulfovibrio* bacteria. *Biochemistry* 47:957–964.
32. Dai SD, Schwendtmayer C, Schürmann P, Ramaswamy S, Eklund H (2000) Redox signaling in chloroplasts: cleavage of disulfides by an iron-sulfur cluster. *Science* 287:655–658.
33. Duin EC, Madadi-Kahkesh S, Hedderich R, Clay MD, Johnson MK (2002) Heterodisulfide reductase from *Methanothermobacter marburgensis* contains an active-site [4Fe-4S] cluster that is directly involved in mediating heterodisulfide reduction. *FEBS Lett* 512:263–268.
34. Walters EM, et al. (2005) Spectroscopic characterization of site-specific $[Fe_4S_4]$ cluster chemistry in Ferredoxin:Thioredoxin Reductase: implications for the catalytic mechanism. *J Am Chem Soc* 127:9612–9624.
35. Dai S, et al. (2007) Structural snapshots along the reaction pathway of Ferredoxin-Thioredoxin Reductase. *Nature* 448:92–96.
36. Niu S, Ichiye T (2009) Probing ligand effects on the redox energies of [4Fe4S] clusters using broken-symmetry density functional theory. *J Phys Chem A* 113:5671–5676.
37. Heering HA, Bulsink YBM, Hagen WR, Meyer TE (1995) Reversible super-reduction of the cubane $[4Fe4S]^{(3+,2+,1+)}$ in the high-potential iron-sulfur protein under non-denaturing conditions—EPR spectroscopic and electrochemical studies. *Eur J Biochem* 232:811–817.
38. Cracknell JA, Wait AF, Lenz O, Friedrich B, Armstrong FA (2009) A kinetic and thermodynamic understanding of O_2 tolerance in [NiFe]-hydrogenases. *Proc Natl Acad Sci USA* 106:20681–20686.